FUNCTIONALLY GRADED INFILL FOR ENHANCED FLEXURAL PERFORMANCE IN 3D-PRINTED PLA

Vishnu Vijayan[1], Abhishek Kottapadikkal Pradeep[1], Harikrishnan Krishnan Muraleedharan[1], Jaymin Vrajlal Sanchaniya[2]
[1]Riga Technical University, Latvia; [2]Kaunas University of Technology, Lithuania
jaymin.sanchaniya@ktu.lt

Abstract. The approach of employing functionally graded infill structures to achieve a more targeted mechanical performance of fused filament fabrication (FFF) components without the corresponding increase in material usage is promising. In this investigation, FFF was used to produce seven polylactic acid (PLA) specimens with different distributions of honeycomb fills in each zone and tested in three-point bending under qualifying ISO 178. Each sample was partitioned into three equal sections where infill density was designated independently on a per-zone basis by either gradient strategy, sandwich strategy and asymmetric strategy in addition to a common uniform 50% infill control. The outer-dense sandwich (S-Out: 80/20/80) exhibited the highest elastic modulus (1753 ± 67 MPa) and the ultimate flexural strength (52.60 ± 0.57 MPa) and the maximum specific flexural strength of 61.4 ± 0.5 $kN \cdot m \cdot kg^{-1}$. These findings establish the importance of the spatial correspondence of infill density to the through-thickness survey of bending stress distribution to determine flexural effectiveness much more than aggregate material content, and that the principles of flexural effectiveness in sandwich composites can be directly applied to zonal FFF infill structure.

Keywords: functionally graded infill, fused filament fabrication, flexural properties, PLA, sandwich structure.

Introduction

In additive manufacturing and fused filament fabrication (FFF) specifically, there has been a swift growth in the number of industries in which it is applied, such as biomedical devices in prototyping [1-3], protective clothing [4-6] to load-bearing structural materials [7-9]. It has enabled FFF to be a compelling platform for both research and engineering applications because of the capability to generate geometrically complex components with controlled internal architecture at low costs [10]. The mechanical behaviour of FFF-printed components is also dependent on a set of process and design factors, extrusion temperature, layer height, raster orientation, and infill structure [11-15]. Of these, the infill pattern and density have a direct effect on structural stiffness and strength, although most of the previous literature has considered infill to be a homogenous, spatially uniform material spread uniformly over an etched component.

Functionally graded materials (FGMs) represent a design technique where composition or structural properties are continuously or discretely varied across a component to allow performance in certain loading conditions to be optimised [16-18]. Flexural behaviour of FGM structures has been further investigated analytically and experimentally, demonstrating the significant role of gradient distribution on bending stiffness and failure [19-21]. The implementation of this concept to FFF infill design makes it possible to control mechanical performance by applying it to isolated locations, avoiding multilateral fabrication and/or post-processing, which is available as part of regular slicing processes.

Past research has shown that tensile mechanical properties of FFF-printed PLA differ significantly between infill patterns with concentric and rectilinear geometries prevailing over less-aligned configurations in modulus and strength [22]. Flexural behaviour has also been studied in terms of infill density, and in most cases, the denser an infill is, the stiffer and stronger it is [23]. Architectures with sandwich composite include have been found to provide high bending stiffness improvements by concentrating material where bending stress is greatest [24]. Nevertheless, little systematic comparison of discrete functionally graded zonal infill strategies under standardised flexural loading can be found when the density is modified across mechanically motivated zones explicitly defined by the three-point bending stress distribution. Most of the earlier gradient investigations have utilised continuously varying density fields or single axis gradients instead of zone-resolved infill assignment.

The current research paper fills this gap by printing and experimenting seven FFF-printed PLA samples where the honeycomb infill density is placed in three equal through thickness zones based on gradient, sandwich, and asymmetric designs. The zone-splitting technique used here is a new and practically available enactment of functional grading in regular FFF slicing equipment, not similar to continuous gradient techniques or multimaterial extrusion.

Materials and methods

All samples were 3D-printed with Prusament PLA filament (Prusa Polymers a.s., Prague, Czech Republic) with a nominal diameter of 1.75 mm as mentioned in [19; 22]. PLA was chosen on its extensively used application in FFF structural prototyping, mechanical behaviour and its application in biomedical and lightweight structural applications. The printing was done using a Prusa Mini FFF printer that had a 0.4 mm nozzle and a glass fibre build plate. Each parameter of the process was held constant within all groups; the entire assortment of circumstances is summarised in Table 1.

Table 1

FFF process parameters were maintained constant across all specimen groups

Parameters	Values
Filament (Ø 1.75 mm)	Prusament PLA
3D Printer	Prusa Mini
Nozzle Diameter (mm)	0.4
Nozzle Temperature (°C)	215
Bed Temperature (°C)	60
Print Speed (mm/s)	25
Layer Height (mm)	0.2
Build Plate	Glass fibre
Infill Pattern	Honeycomb

To determine the effect of the density distribution of the zonal infill on flexural performance during three-point bending, seven specimen configurations were developed. The samples were separated into three equal horizontal segments using the thickness of the sample, and honeycomb fill was added to each segment at densities of 20%, 50%, or 80% of the specimen to create arrangements where the high-density material was aligned or misaligned with the stress gradient created by bending. The density levels of 20%, 50%, and 80% were selected based on engineering judgment to represent low, medium, and high infill extremes, providing a broad comparison range rather than a mathematically optimized distribution. The zone boundaries were defined by the through-thickness bending stress profile, with outer zones corresponding to peak tensile and compressive stress regions and the mid-zone corresponding to the neutral axis. Under three-point bending, tensile and compressive stresses are highest at the bottom and top exterior fibres of the specimen, respectively, and the bending stress decreases to zero at the mid-plane neutral axis. Table 2 presents the seven configurations and includes a uniform control (C-50), two monotonic gradients (G-Up, G-Down), two sandwich (S-Out, S-Inner), and two asymmetric configurations (A-Base, A-Cap). It is a uniquely implemented form of functional grading of continuous density fields and can be entirely realisable in standard FFF slicing software without any hardware variation.

Table 2

Specimen infill configurations with honeycomb density assigned per zone

Sample ID	Description	Infill% (top/mid/bottom)
C-50	Control	50/50/50
G-Up	Gradient (ascending)	20/50/80
G-Down	Gradient (descending)	80/50/20
S-Out	Sandwich (outer-dense)	80/20/80
S-Inner	Sandwich (inner-dense)	20/80/20
A-Base	Asymmetric (base-heavy)	80/20/20
A-Cap	Asymmetric (cap-heavy)	20/20/80

The ISO 178 three-point bending testing was performed on rectangular specimens with dimensions 80 × 10 × 4 mm. Each of the configurations produced 5 replicate samples ($n = 5$) making a total of 35 specimens. The functionally graded infill was implemented as a discrete, layer-wise variation, where each of the three equal through-thickness zones was assigned a fixed honeycomb density (20%, 50%, or 80%), resulting in a stepwise rather than continuous gradient distribution across the specimen thickness. Flexural tests were carried out on a Mecmesin Multi-Test 2.5-i universal testing machine

(PPT Group UK Ltd., Slinfold, UK) using a 250 N load cell, at a cross-head displacement rate of 2 mm·min^{-1} and a support span of 64 mm so that the specific flexural strength could be determined. The results of the mechanical tests, which were obtained after each test, were the flexural modulus (E_f) and the flexural strength (σ_{fM}) as the well as the flexural strain at the flexural strength (ε_{fM}). To calculate the specific flexural strength the mass was measured using the high-precision KERN ABT 5NM analytical balance (resolution 0.000001 g) as detailed in [26-28].

Results and discussion

Table 3 shows the flexural mechanical properties of each of the seven specimen configurations. Fig. 1 shows representative stress(σ)-strain(ε) curves for each configuration. There were significant and systematic configuration-to-configuration variations in elastic modulus, ultimate flexural strength, flexural strain at flexural strength, and specific flexural strength that validate the fact that the spatial distribution of infill density across the specimen thickness has a strong and determinant effect on flexural performance in FFF-printed PLA.

Table 3

Mechanical and physical properties of all specimen configurations

Sample	Flexural modulus E_f, MPa	Flexural strength, σ_{fM}, MPa	Flexural strain at flexural strength ε_{fM}, %	Mass m, g	Specific flexural strength σ_{fM}/ρ, kN·m·kg^{-1}
C-50	1189 ± 30	35.9 ± 1.7	3.96 ± 0.16	2.50 ± 0.01	46.0 ± 1.4
G- Up	1008 ± 34	29.5 ± 0.5	4.34 ± 0.07	2.39 ± 0.01	38.8 ± 0.4
G- Down	1154 ± 14	35.8 ± 1.6	3.98 ± 0.14	2.41 ± 0.01	47.9 ± 1.3
S-Out	1753 ± 67	52.6 ± 0.6	3.86 ± 0.19	2.73 ± 0.01	61.4 ± 0.5
S-Inner	741 ± 32	22.6 ± 0.4	4.37 ± 0.08	2.03 ± 0.01	35.2 ± 0.3
A-Base	1098 ± 19	32.5 ± 0.7	3.78 ± 0.12	2.12 ± 0.01	49.2 ± 0.6
A-Cap	992 ± 27	27.3 ± 0.6	4.22 ± 0.15	2.10 ± 0.01	41.1 ± 0.5

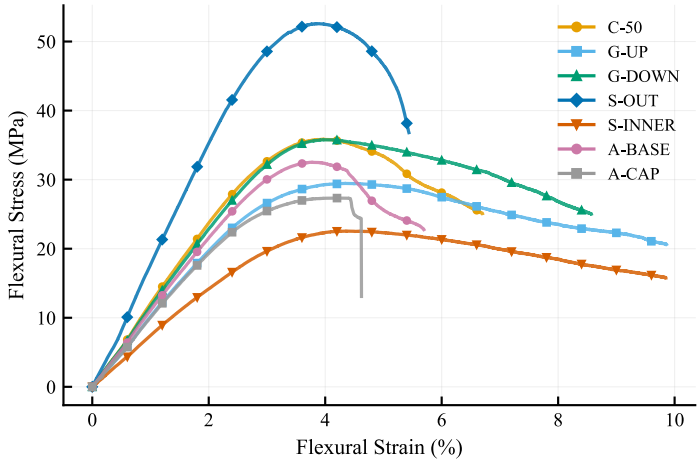

Fig. 1. **Representative curves of flexural stress(σ)–strain(ε) curves for the seven zonal infill**

All specimens remained intact after testing, exhibiting progressive stress reduction beyond peak load, with no observable differences in failure morphology between configurations. The S-Out outer-dense sandwich structure (80/20/80) had the highest elastic modulus (1753 ± 67 MPa) and the ultimate flexural strength (52.60 ± 0.57 MPa) of all the samples tested, which was more than the uniform control C-50 by 47.4 and 46.7%, respectively, in modulus and strength (Table 3). This behaviour can be traced directly to the structural mechanics of sandwich composite design, which places high density (80%) honeycomb fill in the outer zones, which places stiff material where tensile and compressive bending stress is most concentrated, and which places a low density (20%) core in the middle of the section, which contributes little to the resistance to bending but contributes significantly to reduction in the mass

of the middle of the section. The S-Out flexural strength (61.4 ± 0.5 kN·m·kg^{-1}) was the highest of all structures, and was 46.2% higher than the control, indicating the favourable combination of high strength and a more moderate mass increase (2.73 ± 0.01 g, 9.2% higher than the control). Fig. 1 of the stress(σ)-strain(ε) curve of the S-Out has a sharp early slope and a clear maximum stress which is in agreement with the stiff outer layer behaviour before brittle fracture.

Comparing configurations with equal average infill (~47%), S-Out outperformed S-Inner by 132% in the flexural strength, confirming that spatial distribution is the dominant factor over infill percentage alone. The S-Inner (20/80/20) inner-dense sandwich gave the poorest mechanical performance of all reported measures, where the elastic modulus of 741 ± 32 MPa and the flexural strength (σ_{fM}) of 22.57 ± 0.42 MPa; reduces by 37.7% and 37.1% of C-50, respectively (Table 3). This effect is in direct reverse of the rationale of S-Out: by placing high-density infill at the midplane neutral axis, one puts the material under which bending stress is essentially zero, and this causes no contribution to flexural resistance. The compliant outer zones (20% infill) have the highest load of bending but are of low stiffness, which causes early failure. S-Inner also had the lowest specific flexural strength (35.2 ± 0.3 kN·m·kg^{-1}), 23.5% less than the control and 42.7% less than S-Out, although it had the lowest specimen mass of all configurations (2.03 ± 0.01 g, 18.8% less than the control). In this study, the most effective evidence is provided by the juxtaposition of S-Out and S-Inner, which demonstrates that the first factor in flexural structural efficiency is material placement with regard to bending stress gradient rather than total infill volume. Fig. 1 indicates that the stress-strain curve is shallow in slope and low in peak stress, in line with the prevalent effect of the compliant outer zones.

The gradient configurations G-Up (20/50/80) and G-Down (80/50/20) gave intermediate results that correspond to their alignment with bending stress field, respectively. G-Down recorded 1154 ± 14 MPa and 35.79 ± 1.60 MPa of modulus and flexural strength respectively, which are only 2.9% and 0.2% lower than the control, respectively (Table 3), using 3.6% less material. Compared to G-Up (modulus 1008 ± 34 MPa; σ_{fM} 29.47 ± 0.48 MPa) scored 15.2% and 17.8% lower than the control modulus and flexural strength, respectively. By locating the lowest density zone at the tensile face (bottom), the resistance to the tensile bending stress at the maximum tensile bending is reduced significantly, ascertaining that the tensile face plays a considerable role in the flexural rigidity of the short-span bending. G-Down was stronger and better than G-Up by 14.5% in modulus and 21.4% in strength. The flexural strength of G-Down (47.9 ± 1.3 kN·m·kg^{-1}) and G-Up (38.8 ± 0.4 kN·m·kg^{-1}) flexural strength was 4.1% higher and 15.7% lower than the control, respectively, which means that the direction of the gradient is not insignificant when it comes to mass efficiency. The flexural strain at the flexural strength (ε_{fM}) in both gradient designs was slightly higher than that of the control (G-Up: 4.34%; G-Down: 3.98% vs C-50: 3.96%), indicating that compliance in the regions of lower stiffness was slightly improved.

The asymmetric designs A-Base (80/20/20) and A-Cap (20/20/80) had high-density fill only in one of the outer zones, and infill in the other two areas was 20%. A-Base registered a modulus of 1098 ± 19 MPa and a flexural strength of 32.54 ± 0.72 MPa and A-Cap registered lower values of 992 ± 27 MPa and 27.35 ± 0.59 MPa, 10.7% variation in modulus and 19.0% strength in favour of A-Base (Table 3). The mass of both asymmetric specimens was significantly lower compared to the control (A-Base: 2.12 g, -15.2%; A-Cap: 2.10 g, 16.0%), but their respective specific flexural strength was different: A-Base got 49.2 ± 0.6 kN·m·kg^{-1} (+7% versus control) and A-Cap only 41.1 ± 0.5 kN·m·kg^{-1} (-10.7% versus C-50). The better performance of A-Base than A-Cap with the same average infill content indicates that in three-point bending geometry, compressive face (top zone) rather than tensile face (bottom zone) of the same density has a measurable effect on flexural stiffness. These two designs were worse than C-50 in absolute mechanical terms, and A-Base showed that single-face densification provides an effective intermediate solution - it is possible to decrease the specimen mass by more than 15% without incurring excessive penalty in terms of the specific flexural strength.

The range of the specific flexural strength of all samples is 35.2 to 61.4 kN·m·kg^{-1}, and the difference in the specific flexural strength between the worst (S-Inner) and the best (S-Out) is 74.4%, which supports the extent of improvement that can be achieved only by informed zonal infill design.

Conclusions

1. The seven zonal honeycomb infill structures in FFF-printed PLA were tested in ISO 178 three-point bending. The outer dense sandwich S-Out (80/20/80) had the largest elastic modulus (1753 ± 67

MPa) and the ultimate flexural strength (52.60 ± 0.57 MPa), which is 47.4% and 46.7% higher than that of the control, respectively. S-Inner (20/80/20), on the other hand, gave the worst results; 37.7% and 37.1% poorer in modulus and strength, respectively, than the control material which means that flexural efficiency depends more on stress aligned material placement rather than total infill volume.

2. There was also a 74.4% difference in the flexural strength depending on all samples (35.2 to 61.4 $kN \cdot m \cdot kg^{-1}$), indicating that zone-resolved infill assignment is a promising and readily available approach to flexural maximisation in FFF. Future studies are needed to investigate the number of zones, the ratio of thickness, and other fill patterns, and expand the work to the biomedical and structurally loaded components. Future work should extend zonal infill investigations to engineering-grade polymers such as ABS and PEEK to broaden applicability.

Author contributions:

V.V. and J.V.S.: conceptualization, methodology, validation, visualization, project administration; V.V.: software, investigation, data curation, writing – original draft, funding acquisition; A.K.P. and A.K.P.: software, investigation, data curation; J.V.S.: writing – review and editing. All authors have read and agreed to the published version of the manuscript.

References

[1] Mitchell K., Shackleford A., Bandala E., Zhang C., Chai G., Jin Y. Embedded Fused Filament Fabrication of Thermoplastics for Biomedical Applications, J. Manuf. Sci. Eng., vol. 147, no. 6, 2025, DOI: 10.1115/1.4067865

[2] Kumar A., Cheshta, Avinash, Mir T. H., Mursaleen M., Shah M. A. Innovative scaffold design in biomedical: a comprehensive review of biomaterial integration and 3D printing techniques with emphasis on fused filament fabrication, Int. J. Pharm., vol. 685, 2025, p. 126250, DOI: 10.1016/j.ijpharm.2025.126250

[3] Kothandaraman L., Balasubramanian N. K., Palaniyappan S., Dalaq A. S., Bodaghi M. Material extrusion techniques for biomedical applications: Biomaterials and their performance - A review, Mater. Today Commun., vol. 49, 2025, p. 113707, DOI: 10.1016/j.mtcomm.2025.113707

[4] Vejanand S. R., Janushevskis A., Vaicis I. Selection of Appropriate Estimation Criteria in Flow Simulation Study for Predicting Cooling Efficiency of Ventilated Protective Clothing, Latv. J. Phys. Tech. Sci., vol. 62, no. 2, 2025, pp. 17-29, DOI: 10.2478/lpts-2025-0010

[5] Yu M., Ke B. Development and compressive performance study of 3D printing auxetic structure-Spacer fabric composites, Int. J. Cloth. Sci. Technol., vol. 37, no. 5, 2025, pp. 1006-1021, DOI: 10.1108/IJCST-09-2024-0193

[6] Zolfagharian A., Català G. B., Saakes D., Rolfe B., Gibson I., Mehrpouya M. 3D-Printed Architected Material for the Generation of Foam-Based Protective Equipment, Adv. Eng. Mater., vol. 27, no. 21, 2025, p. 2500132, DOI: 10.1002/adem.202500132

[7] Ram, Mane S., Shaheen H., Ramaiah G. B. Enhancing the structural integrity and load-bearing capacity of 3D-printed ABS polymer materials using innovative approach, Prog. Addit. Manuf., vol. 10, no. 12, 2025, pp. 11131-11146, DOI: 10.1007/s40964-025-01278-z

[8] Dhanapal R., Alagumalai V., Shanmugam V. Exploring the dynamic mechanical properties of fused filament fabrication printed polyetheretherketone with various infill patterns, Prog. Addit. Manuf., vol. 10, no. 4, 2025, pp. 2911-2926, DOI: 10.1007/s40964-024-00792-w

[9] Kantaros A., Drosos C., Papoutsidakis M., Pallis E., Ganetsos T. Composite Filament Materials for 3D-Printed Drone Parts: Advancements in Mechanical Strength, Weight Optimization and Embedded Electronics, Materials, vol. 18, no. 11. p. 2465, 2025. DOI: 10.3390/ma18112465

[10] Gupta V., Bankapalli N. K., Saxena P., Bajpai A., Ruan D. Additive Manufacturing of Fiber-Reinforced Polymer Matrix Composites through Material Extrusion: A Comprehensive Review on Filament Fabrication, Printing, Testing Methods, Applications, and Challenges, Adv. Eng. Mater., vol. n/a, no. n/a, 2025, p. 2500676, DOI: 10.1002/adem.202500676

[11] Raj A., Tyagi B., Sharma G. S., Sahai A., Sharma R. S. Optimizing the process parameters with statistical and soft computing techniques for enhanced mechanical properties of acrylonitrile

butadiene styrene material samples fabricated via fused filament fabrication technique, Prog. Addit. Manuf., vol. 10, no. 4, 2025, pp. 2559-2583, DOI: 10.1007/s40964-024-00767-x
[12] Umer M. H. et al. Influence of process parameters on mechanical properties and surface roughness in fused filament fabrication: a comprehensive review, J. Brazilian Soc. Mech. Sci. Eng., vol. 47, no. 6, 2025, p. 259, DOI: 10.1007/s40430-025-05579-w
[13] Kumar P., Patel R., Singh I., Agrawal S., Kechagias J. D. Optimising the fused filament fabrication process employing the experimental design approach: An expository paradigm under cold weather conditions and lightweight specimens, Next Mater., vol. 7, 2025, p. 100387, DOI: 10.1016/j.nxmate.2024.100387
[14] Thotakuri M., Yelamasetti B., I. S. S. P., Sk M. S., P. N. K. Process parameter optimization of fused filament fabrication - 3D printing with PETG: a multi-objective approach using the matrix method, Rapid Prototyp. J., vol. 32, no. 3, 2025, pp. 799-820, DOI: 10.1108/RPJ-12-2024-0529
[15] Gajjar T., Yang R. (Chunhui), Ye L., Zhang Y. X. Effects of key process parameters on tensile properties and interlayer bonding behavior of 3D printed PLA using fused filament fabrication, Prog. Addit. Manuf., vol. 10, no. 2, 2025, pp. 1261-1280, DOI: 10.1007/s40964-024-00704-y
[16] Li Kun et al. High performance realization of functionally graded materials based on integrated optimal design and additive manufacturing: A review, Int. Mater. Rev., vol. 70, no. 6, 2025, pp. 497-547, DOI: 10.1177/09506608251354889
[17] Ghanavati R. et al. Design optimization for defect-free AISI 316 L/IN718 functionally graded materials produced by laser additive manufacturing, Mater. Charact., vol. 220, 2025, p. 114697, DOI: 10.1016/j.matchar.2024.114697
[18] Jain R. et al. Functionally Graded Metallic Materials Via Additive Manufacturing: Research Progress on Processing, Challenges, and Applications, Int. J. Precis. Eng. Manuf. Technol., vol. 13, no. 1, 2026, pp. 281-328, DOI: 10.1007/s40684-025-00766-5
[19] Njim E. K., Sadiq S. E., Tahir M. S. A. D., Flayyih M. A., Hadji L. Flexural bending and fatigue analysis of functionally graded viscoelastic materials: experimental and numerical approaches, Phys. Chem. Solid State, vol. 24, no. 4, 2023, pp. 628-639, DOI: 10.15330/pcss.24.4.628-639
[20] Hu J., Dong P., Hou R., Cao J., Sadeghzade S., Yuan H. Functionally graded IWP reinforced cementitious composites: Design, fabrication, and the enhanced ductility, Thin-Walled Struct., vol. 192, 2023, DOI: 10.1016/j.tws.2023.111199
[21] Xu Y., Zhang H., Gan Y., Šavija B. Cementitious composites reinforced with 3D printed functionally graded polymeric lattice structures: Experiments and modelling, Addit. Manuf., vol. 39, 2021, DOI: 10.1016/j.addma.2021.101887
[22] Sanchaniya J. V, Kannathasan K. R., Vejanand S. R., Joshi J., Lasenko I. Effect of Infill Pattern Design on Tensile Strength of Fused Deposition Modelled Specimens, Environment Technology Resources - Proceedings of the 16th International Scientific and Practical Conference, 2025, vol. 4, pp. 375-382. DOI: 10.17770/etr2025vol4.8409
[23] Buss C., Reci F., Hribernig T., Steininger S. Experimental Investigation into the Influence of Infill Density, Print Pattern, and Built-Up Direction on the Flexural Strength of FFF-Manufactured PLA Components, Journal of Manufacturing and Materials Processing, vol. 10, no. 1. p. 21, 2026. DOI: 10.3390/jmmp10010021
[24] Guerra Silva R., Morales Pavez G. Flexural characteristics of additively manufactured continuous fiber-reinforced honeycomb sandwich structures, Compos. Part C Open Access, vol. 16, 2025, p. 100563, DOI: 10.1016/j.jcomc.2025.100563
[25] Sanchaniya J. V, Smogor H., Gobins V., Noël V., Lasenko I., Rackauskas S. Layer-by-Layer Integration of Electrospun Nanofibers in FDM 3D Printing for Hierarchical Composite Fabrication, Polymers (Basel)., vol. 18, no. 1, 2026, DOI: 10.3390/polym18010078
[26] Sanchaniya J. V. et al. A Novel Method to Enhance the Mechanical Properties of Polyacrylonitrile Nanofiber Mats: An Experimental and Numerical Investigation, Polymers (Basel)., vol. 16, no. 7, 2024, p. 992, DOI: 10.3390/polym16070992
[27] Sanchaniya J. V Comparative Analysis of Thermal Characteristics: Virgin Polyacrylonitrile (PAN) versus Electrospun PAN Nanofibre Mats, Latv. J. Phys. Tech. Sci., vol. 61, no. 4, 2024, pp. 98-105, DOI: 10.2478/lpts-2024-0031
[28] Sanchaniya J. V. et al. Mechanical and thermal characteristics of annealed-oriented PAN nanofibers, Polymers (Basel)., 2023, DOI: doi.org/10.3390/polym15153287